13 C-Isotopomer-based metabolomics of microbial groups isolated from two forest soils

ARTICLE *in* METABOLOMICS · MARCH 2009

Impact Factor: 3.86 · DOI: 10.1007/s11306-008-0150-2

3 AUTHORS:

Teresa Fan
University of Louisville
59 PUBLICATIONS **2,379** CITATIONS
SEE PROFILE

Jeffrey A. Bird
City University of New York - Queens College
55 PUBLICATIONS **868** CITATIONS
SEE PROFILE

Eoin L Brodie
Lawrence Berkeley National Laboratory
142 PUBLICATIONS **9,010** CITATIONS
SEE PROFILE

Metabolomics (2009) 5:108–122
DOI 10.1007/s11306-008-0150-2

ORIGINAL ARTICLE

^{13}C-Isotopomer-based metabolomics of microbial groups isolated from two forest soils

Teresa W.-M. Fan · Jeffrey A. Bird · Eoin L. Brodie · Andrew N. Lane

Received: 10 July 2008 / Accepted: 10 December 2008 / Published online: 28 December 2008

Abstract Soil microorganisms are the primary mediators of organic matter decomposition and humification processes in soil, which represent a critical C flux in the global C cycle. Little is known about how soil microbes regulate carbon cycling including the contribution of their own biomass to stable soil organic matter. A comprehensive understanding of microbial composition is a first step to unraveling microbial regulation of soil humification processes. For this purpose, we isolated 23 microbial strains representing four major groups (Gram (+) bacteria, Gram (−) bacteria, Actinobacteria, and Fungi) from a temperate and a tropical forest soil. The microbial isolates were cultured with uniformly ^{13}C-labeled glucose as the C source such that all biochemical components synthesized from glucose were ^{13}C labeled. This approach enabled field mesocosm experiments on tracking microbial decomposition, while facilitating solution- and solid-state NMR analysis of microbial composition. Polar and lipid extracts of labeled biomass of the four microbial groups from the two forest sites were profiled by 2D NMR methods, including high-resolution heteronuclear single quantum coherence spectroscopy and HCCH-total correlation spectroscopy. This ^{13}C labeling approach also enabled the analysis of intact biomass by 2D solid-state ^{13}C–^{13}C correlation spectroscopy. Distinction between microbial groups and sites was observed in the polar and lipophilic metabolite profiles. Dominant differences could also be related to the capacity for lipid β-oxidation or adaptation to desiccation. Solid-state NMR further revealed differential synthetic capacity for glycolipids among groups. This technology coupled with ^{13}C metabolite profiling should facilitate future functional annotation of indigenous microbial genomes.

Keywords 2D solution-state NMR · 2D solid-state ^{13}C NMR · Gram negative bacteria · Gram positive bacteria · Actinobacteria · Fungi

Abbreviations

BHT	Butylated hydroxytoluene
DSS	2,2′-Dimethylsilapentane-5-sulfonate
EPS	Extracellular polysaccharide
HSQC	Heteronuclear single quantum coherence
TOCSY	Total correlation spectroscopy

1 Introduction

Understanding soil organic matter (SOM) dynamics is critical to meeting many environmental, agricultural, and forestry challenges relating to productivity and sustainability, including the potential of soils to sequester atmospheric CO_2, control net ecosystem production (NEP),

T. W.-M. Fan (✉) · A. N. Lane
Center for Regulatory and Environmental Analytical Metabolomics (CREAM), Department of Chemistry, University of Louisville, 2210 S. Brook St., Belknap Research Building, Rm 348, Louisville, KY 40208, USA
e-mail: teresa.fan@louisville.edu; twmfan@gmail.com

T. W.-M. Fan · A. N. Lane
James Graham Brown Cancer Center, University of Louisville, Louisville, KY 40202, USA

J. A. Bird
School of Earth and Environmental Sciences, Queens College, City University of New York, Flushing, NY 11367, USA

E. L. Brodie
Earth Sciences Division, Ecology Department, Lawrence Berkeley National Laboratory, Berkeley, CA 94720, USA

and support production of food and fiber. The amount of C as SOM (ca. 1400–1500 Pg C) represents two-thirds of the terrestrial C pool (Eswaran et al. 1993; Post et al. 1982; Schlesinger 1977) and is the primary energy source driving soil biogeochemical processes. While soil microorganisms are known to be the primary mediators of decomposition and humification processes in terrestrial environments, little information exists on how microbes regulate the conversion of plant material into humic substances. An often-overlooked influence of soil microorganisms on C stabilization processes is that their bodies, or biomass, are primary building blocks in the formation of SOM (Kögel-Knabner 2002). Researchers are now recognizing how soil C cycling processes are affected by soil microbial community structure (Meyers et al. 2001; Saetre and Bååth 2000; Waldrop and Firestone 2003). It is, however, often not recognized that soil microbial biomass comprises a primary step in the sequence of humification by providing a significant reservoir of building blocks for the formation of humic substances. If the structure of the microbial community determines the biochemistry of microbial biomass, and these bodies are primary precursors of humic substances, then microbial community composition will influence the amount and stability of humified C.

To characterize comprehensively the biochemical composition of microbial communities, we have taken a ^{13}C-isotopomer-based metabolomic approach, which we have employed previously in delineating mammalian metabolic networks in response to stressors (Fan et al. 2005, 2006) and in characterizing soil humic structures (Fan et al. 2004). This approach utilizes uniformly labeled ^{13}C-glucose as a tracer for culturing representative classes of microbes isolated from field sites such that all metabolites that are derived from glucose become labeled. This enables the use of a wider array of NMR techniques for profiling microbial components than what is practical with very limited biomass. These include, but not limited to, 2D ^{1}H–^{13}C high-resolution heteronuclear single quantum coherence spectroscopy (HR-HSQC), 1D solid-state cross-polarization magic angle spinning (CP-MAS) ^{13}C NMR, and 2D solid-state CP-MAS ^{13}C–^{13}C correlation spectroscopy. The solution-state HR-HSQC analysis reveals ^{13}C spin coupling information to facilitate metabolite assignment in microbial extracts while the latter two solid-state ^{13}C NMR analyses allows in situ characterization of microbial components that may not be readily extracted. This represents a substantial technical development for the analysis of global metabolic potential in environmental microbes.

More importantly, the ^{13}C-labeled isotopomer profiles obtained can have important functional implications. First, it is reasonable to assume that all labeled metabolites are synthesized from the labeled precursor by definable pathway(s). Accordingly, each labeled profile can serve as a fingerprint of active metabolic networks. Such fingerprint may be utilized for functional classification of microbial communities. Second, it would be feasible to reconstruct pathway scenarios based on ^{13}C-labeled isotopomer profiles and existing microbial metabolic databases (e.g. http://www.metacyc.org), thereby revealing relevant genes that may be functionally expressed. This knowledge should be valuable towards building understanding in the functional genomics of microbial community involved in a wide range of environmental processes including the genesis and decomposition of SOM.

Specifically, the microbial isolates examined in this study are being used to test whether differences in the chemical composition of microbial biomass, and thereby microbial community composition, can be related to the quantity and quality of the SOM produced from their biomass. The biochemical fingerprints of the isolates obtained in this report will also be utilized to identify key characteristics of the microbial community that influence humification processes and their products, thereby enhancing our understanding of the mechanisms involved in C stabilization and sequestration in terrestrial environments.

2 Materials and methods

2.1 Microbial isolation and culturing

We isolated 23 microbial strains which were categorized in four cell-type groups, i.e. 2–4 isolates each of (1) Gram positive (+) bacteria, (2) Gram negative (−) bacteria, (3) Actinobacteria and (4) Fungi, from a temperate coniferous and a tropical wet forest soils sampled in 2004 (cf. Table 1). These groups of isolates allowed for comparison of the four main morphological types of soil microorganisms. At each forest site, soil samples were taken (0–15 cm depth) at 15 locations along 3 transects and homogenized separately. These samples were maintained at field moisture and ambient temperature before subsampling for culturing within 4 d in the laboratory. The tropical forest site is located near Luquillo, Puerto Rico (18°17′N, 65°47′W) at an elevation of 780 m. Mean annual precipitation is 420 cm and mean annual temperature is 19.5°C at the tropical forest site. The tropical soil is a sandy loam, Humic Dystrudept (Staff 1999). The dominant plant species at the tropical site is *Cyrilla racemiflora*. The temperate forest site is located near Georgetown, CA (38°54′N, 120°39′W) at an elevation of 1288 m. Mean annual precipitation at the temperate site was 166 cm and mean annual temperature was 11.0°C. The temperate soil is a sandy loam, Ultic Haploxeralf (Soil Survey Staff 1999).

Table 1 Classification and properties of microbial isolates from two forest sites

Taxonomic group	Cell-type group	Genus/species of closest BLAST match isolate	Best BLAST match[a]	Mass in group[b] (%)	SUE[c] (%)	EPS[d] (%)
Ascomycete	Fungal	*Penicillium sacculum*	AB031391.1	78.2	11.3	2.8
Basidiomycete (mycelial)	Fungal	*Cryptococcus* sp.	AY749434.1	8.8	2.2	2.9
Basidiomycete (yeast)	Fungal	*Cryptococcus phenolicus*	AF444351.1	6.2	3.0	7.1
Zygomycete	Fungal	*Umbelopsis* sp.	AY376409.1	6.9	1.3	1.4
Streptomycetaceae	Actinobacteria	*Streptomyces* sp.	EF524057.1	28.3	1.5	0.8
Streptomycetaceae	Actinobacteria	*Streptomyces* sp.	AJ308572.1	51.7	1.6	4.1
Streptomycetaceae	Actinobacteria	*Streptomyces capoamus*	AB045877.1	20.0	2.6	7.3
Actinobacteria (non-Streptomycetaceae)	High-GC Gram positive	*Arthrobacter methylotrophus*	AF235090.1	68.7	1.2	17.3
Firmicutes	Low-GC Gram positive	*Bacillus subtilis*	AY030331.1	31.3	3.7	15.5
Alpha-proteobacteria	Gram negative	*Rhizobium* sp.	U89823.1	37.7	1.9	17.7
Beta-proteobacteria	Gram negative	*Burkholderia* sp.	AY949194.1	37.5	4.0	0.1
Beta-proteobacteria	Gram negative	*Burkholderia* sp.	AY178062.1	24.9	2.1	10.5
Ascomycete	Fungal	*Penicillium pinophilum*	AB369480.1	87.4	3.9	0.0
Basidiomycete (mycelial)	Fungal	*Trichosporon multisporum*	AB001764.2	9.6	2.9	3.7
Basidiomycete (yeast)	Fungal	*Cryptococcus podzolicus*	AB032645.1	3.0	4.3	2.8
Streptomycetaceae	Actinobacteria	*Kitasatospora griseola*	U93320.1	35.1	2.1	0.7
Streptomycetaceae	Actinobacteria	*Kitasatospora arboriphila*	AY442267.1	29.1	4.2	42.5
Streptomycetaceae	Actinobacteria	*Streptomyces* sp.	AB366323.1	35.8	3.7	1.0
Firmicutes	Low-GC Gram positive	*Bacillus mycoides*	AB116121.1	40.0	0.8	16.8
Firmicutes	Low-GC Gram positive	*Bacillus* sp.	DQ854981.1	60.0	0.5	5.3
Beta-proteobacteria	Gram negative	*Burkholderia plantarii*	AB183678.1	76.8	3.2	11.3
Gamma-proteobacteria	Gram negative	*Dyella* sp.	EU604273.1	21.1	2.8	6.8
Bacteroidetes	Gram negative	*Chitinophaga* sp.	AB278570.1	2.1	1.8	1.4

Isolates derived from Luquillo Puerto Rico (wet tropical) and Georgetown, California (temperate, coniferous), respectively

[a] Accession number of top BLAST match (as of August 2008)

[b] Proportion of a given species (expressed as a percent) in a site specific cell-type group

[c] Substrate use efficiency (SUE): percent of microbial biomass (and EPS) C produced at late stationary phase (harvest) relative to the glucose C provided

[d] Percent of extracellular polysaccharide (EPS) C produced relative to total biomass C of a given species

The dominant species at the temperate site was *Pinus ponderosa*.

The initial culturing procedures screened hundreds of isolates per site and was performed using soil-extract amended agar with 10% trypticase soy agar (TSA) or trypticase soy broth (TSB) at pH 5.5 (Alef 1995). Cultures within each cell type group were further isolated using additions to the media of starch casein or chitin with cyclohexamide (50 mg l^{-1}) for Actinobacteria, 10% TSA with cyclohexamide (50 mg l^{-1}) for Gram (+) and Gram (−) bacteria and potato dextrose agar (PDA) with streptomycin (100 g l^{-1}) and novobiocin (45 mg l^{-1}) for Fungi (Alef 1995). Final selections were intended to produce a diverse group of isolates within each cell-type group. Preliminary "candidate" isolates were screened for robust growth using liquid media to ensure availability of sufficient labeled biomass for field experimentation. Liquid media used for growth assessment was glucose (1.53%) with M9 salts at pH 5.5 (Alef 1995). A final selection of 23 isolates was made and their identity confirmed. DNA was extracted from all isolates using commercially available extraction kits (PowerSoil, Mobio Inc, CA). For identification of bacterial isolates 16S rRNA genes were amplified using "universal" primers 27F and R1492 (Lane et al. 1985). For Fungal characterization the 18S-5.8S-28S ITS regions were amplified using primers ITS1F and ITS4 (Gardes and Bruns 1993). Amplified rRNA gene and ITS sequences were digested with restriction endonucleases, and subsequent banding patterns were used to organize isolates into OTUs. Full sequences (i.e. forward and

reverse) were obtained by dideoxy terminator sequencing at the UC Berkeley Sequencing Center and base-called and assembled using "phred" and "phrap" respectively. High quality sequences (phred score $q \geq 20$) were compared with public databases including NCBI Genbank and greengenes (DeSantis et al. 2006) by BLAST and alignments were performed to determine the phylogenetic distance among isolates. Based on these data, we selected 2–4 diverse members from the Gram (−) bacteria, high and low-GC Gram (+) bacteria, Actinobacteria, and Fungal groups for liquid medium culturing for each site for a total of 8 groups. Phylogenetic details of each isolate are shown in Table 1.

The final 23 isolates selected were grown in liquid media amended with glucose (1.53%, unlabeled or uniformly ^{13}C-labeled to >99 at.%, CIL, MA) and yeast extract (10%) with M9 salts at pH 5.5 (Alef 1995). Uniformly enriched glucose accounted for least 99% of carbon in the medium. The remaining C was unlabeled yeast extract (0.43%; EM Science, Gillstown, NY) provided to isolates during the early culture stage (i.e. 8-ml culture). Isolates were grown to late stationary phase in 1 L culture flasks at 25°C. Approximately 1 g cell material (dry matter) was produced for each of the 23 isolates for biochemical analyses and soil amendment. Whole cells were harvested by centrifugation and subsequently washed with phosphate buffer solution (0.1 M, pH 7.0) to remove media components. Cell exudates produced during culturing (extra-cellular polysaccharides (EPS) and low-density cellular material) not isolated with the cells by centrifugation were concentrated using 0.1-μm polycarbonate filters (Sterlitech Co., Kent, WA) from the used media and washed with deionized water. Cells and concentrated EPS were sterilized by autoclaving for two 30-min cycles at 121°C. This procedure was required for field deployment of cultured isolates and may damage heat-labile components including some amino acids and vitamins. After autoclaving, isolate cells and EPS were lyophilized and homogenized. Isolates and their EPS were subsampled and combined in proportions as in Table 1 into temperate and tropical version of the 4 cell-type groups: (1) Gram positive (+) bacteria, (2) Gram negative (−) bacteria, (3) Actinobacteria and (4) Fungi for subsequent analyzes and field application. Microbial biomass was analyzed by isotope ratio MS, and the ^{13}C enrichment was >95% for all isolates (Table 1). The ^{13}C enrichment was confirmed for metabolites in microbial group extracts and in situ by ^{13}C NMR analysis (see below) and implied that the signal intensity in ^{13}C spectra represents actual metabolic abundance in the sample.

The C utilization efficiency and the proportion of EPS produced during culture varied significantly among isolates (Table 1). The inclusion of EPS and low-density cellular material with the addition of whole, dead cells to soils will provide a more complete assessment of the biochemical composition and fate of microbial C products formed by different cell-type groups. No research known to date has included microbial exudates (EPS) along with cell mass for their biochemical profiling and degradation dynamics in soil. The latter study is ongoing and will be reported elsewhere.

2.2 Sample extraction

For extracting polar metabolites, 5–8 mg of lyophilized microbial biomass from each cell-type group was homogenized in 60% acetonitrile (w/v 100/1) with glass beads (3 mm in diameter, Fisher Scientific, Pittsburgh, PA) in a micro-ballmill (MM200, Retsch, Inc., Newtown, PA) for 1 min at 30 Hz. The homogenate was kept at −80°C for 30 min before centrifugation at 2,08,000*g* for 20 min at 4°C. After removing the supernatant, the pellet was washed in 60% acetonitrile and processed as described above but without the −80°C storage step. The two supernatants were pooled, lyophilized, and stored at −80°C until NMR analysis. The lipid extracts were prepared similarly as the polar extracts except that methanol containing 1 mM butylated hydroxytoluene (BHT as anti-oxidant) was used as the extraction solvent and the homogenate was nutated at room temperature for 1 h before centrifugation. The methanolic extract was dried in a Speedvac (Vacufuge™ 5301, Eppendorf, Westbury, NY), redissolved in 0.5 ml methanol plus BHT, and stored at −80°C until NMR and MS analysis.

2.3 NMR analysis

The lyophilized polar extracts were dissolved in 0.35 ml D_2O plus 30 nmol of deuterated DSS (2,2-dimethyl-2-silapentane-5-sulfonic acid-D_6, Sigma–Aldrich, St. Louis, MO) and loaded into a Shigemi NMR tube (Shigemi, Inc., Allison Park, PA). 1D ^{1}H NMR of the extracts was performed on an 18.8 T Inova NMR spectrometer (Varian, Inc., Palo Alto, CA) at 20°C in a 5-mm HCN triple resonance pfg probe, using a PRESAT pulse sequence for residual HOD saturation, a 90° pulse, 2 s acquisition time, and 5 s recycle time. 2D ^{1}H TOCSY (total correlation spectroscopy), ^{1}H HCCH-TOCSY, and ^{1}H–^{13}C HSQC (heteronuclear single quantum coherence spectroscopy) of the extracts were also acquired at 18.8 T using gradient-based pulse sequences available in the Varian software. The acquisition parameters for the 2D experiments are listed in Table 2.

The lipid extracts in methanol were dried in the Vacufuge™ before redissolution in 0.36 ml methanol-d_4 (Cambridge Isotope Laboratories, Andover, MA) and

Table 2 NMR acquisition parameters for various 2D experiments

2D experiment	t_2 (s)[a]	t_1 (s)[a]	Interpulse delay (s)	np[b]	np2[b]
TOCSY	0.293	0.032	1.7	4683	256
HCCH-TOCSY	0.140	0.05	1.5	1960	350
HSQC (D_2O)	0.14	0.021	1.5	2240	512
HSQC (methanol-d_4)	0.12	0.028	1.5	1440	512

[a] t_2 and t_1 are acquisition times in the 1st and 2nd dimensions, respectively

[b] np and np2 are number of digital points in the 1st and 2nd dimensions, respectively

loading into Shigemi tubes. 1D ^{1}H NMR of the extracts were performed on a 14.4 T Inova NMR spectrometer at 20°C in a 5-mm HCN triple resonance pfg coldprobe, using a PRESAT pulse sequence for residual methanol saturation, 90° pulse, 2 s acquisition time, and 5 s recycle time. 2D ^{1}H–^{13}C HSQC of the extracts was also acquired at 14.4 T using the gradient-based pulse sequence available in the Varian software and acquisition parameters listed in Table 2.

Intact microbial biomass (17–20 mg) from each cell-type group was loaded into a thin-walled 3 mm rotor. Solid-state NMR spectra of the biomass were recorded on an 18.8 T (201.1 MHz for ^{13}C) Varian Inova NMR spectrometer. The rotor was spun at the magic angle speed ranging from 6 to 10 kHz at ambient temperature (20°C). Optimization of the magic angle was carried out using KBr, and shimming of the ^{13}C signal was optimized using a sample of adamantane (Taylor 2004). The ^{13}C line width of adamantane was routinely <10 Hz under MAS conditions. ^{13}C cross polarization magic angle spinning (CP-MAS) spectra were recorded on a triply tuned 3.2 mm HCN MAS probe. For 1D spectra, a ramped cross polarization scheme was used to match the ^{1}H and ^{13}C power levels, with optimization both of the contact time (6 ms) and the recycle time (2 s) of the experiment. Other spectral parameters included 90° proton pulse of 5.5 μs, acquisition time of 50 ms, and spectral width 100 kHz.

As ^{13}C–^{13}C scalar couplings were resolved in the solid-state 1D NMR spectra for some resonances, we performed a 2D scalar correlation experiment (^{13}C–^{13}C TOCSY) to identify spin systems, using a sequence provided by Varian. The carbons were cross-polarized from the proton reservoir as in the 1D experiment, followed by a CPMG spin lock. The carbon pulse widths were carefully calibrated to optimize the signal (90° pulse width = 1.75 μs). 300 complex pairs of t_1 increments were recorded, for a $t_1$max of 6 ms. A CP contact of 6 ms was used with the spin-lock duration varied from 8 to 15 ms, corresponding to $1/2J_{CC}$ values for aliphatic carbons.

3 Results and discussion

3.1 Polar metabolites in extracts

Polar extracts of ^{13}C-labeled biomass from the microbial cell-type groups of each forest soil were analyzed by 1D and 2D NMR analysis. Figure 1 shows the 2D ^{1}H NMR analysis of the Actinobacteria extract for the California site. The ^{1}H total correlation (TOCSY) spectrum (Fig. 1a) traced the proton covalent linkages (represented by the off-diagonal cross-peak patterns) within a metabolite's molecular framework. Since all metabolites were almost entirely enriched in ^{13}C (see Sect. 2), each pair of ^{1}H cross-peaks showed the characteristic doubly ^{13}C labeled pattern ( ) as traced by dashed rectangles, resulting from the coupling between the proton and the directly attached ^{13}C atom (i.e. ^{13}C satellites) (Fan and Lane 2008; Lane et al. 2008; Lane and Fan 2007). The chemical shifts of the protons attached to ^{12}C used for metabolite assignment were calculated from the center of the split cross-peaks. These chemical shift values were confirmed in the corresponding HCCH-TOCSY spectrum of the same extract, where the ^{1}H chemical shifts assumed those of the ^{12}C-attached protons.

The overall cross-peak patterns in Fig. 1a indicate that most, if not all, metabolites were fully labeled in ^{13}C, in agreement with the isotope ratio MS data of the whole cells (see Sect. 2). This demonstrates that the synthesis of these metabolites using carbon from the supplied [U-^{13}C]-glucose. These include amino acids (Leu, Val, Thr, Ala, Lys, Arg, Glu, Gln, Asp, Tyr, Phe), organic acids (β-hydroxybutyrate), sugars (trehalose), and nucleotides (ATP and UTP). The full ^{13}C enrichment in these metabolites was also evident in the 2D ^{1}H HCCH-TOCSY contour map of the same extract, as shown in Fig. 1b. Only protons that were attached to consecutively ^{13}C labeled carbons gave rise to off-diagonal cross-peaks in this spectrum. Thus, the cross-peak patterns for the above metabolites in the HCCH-TOCSY spectrum confirmed the ^{13}C enrichment pattern in the TOCSY spectrum (Fig. 1a). The 2D NMR analysis enabled conclusive assignment of the ^{1}H resonances in the corresponding highly overlapping 1D ^{1}H NMR spectra (in part due to additional ^{13}C satellite resonances), as shown in Fig. 1.

Once assigned, the 1D ^{1}H NMR spectra of the crude extracts enabled a global comparison of polar metabolite profiles for 4 each microbial groups from the two field sites. To reduce the spectral crowding due to the presence of ^{13}C satellites, 1D ^{1}H NMR spectra of the unlabeled microbial extracts with no observable ^{13}C satellites are used, as shown in Fig. 2. It is clear that the biochemical composition of these extracts exhibited both similarities and differences. The polar metabolite profiles of the four

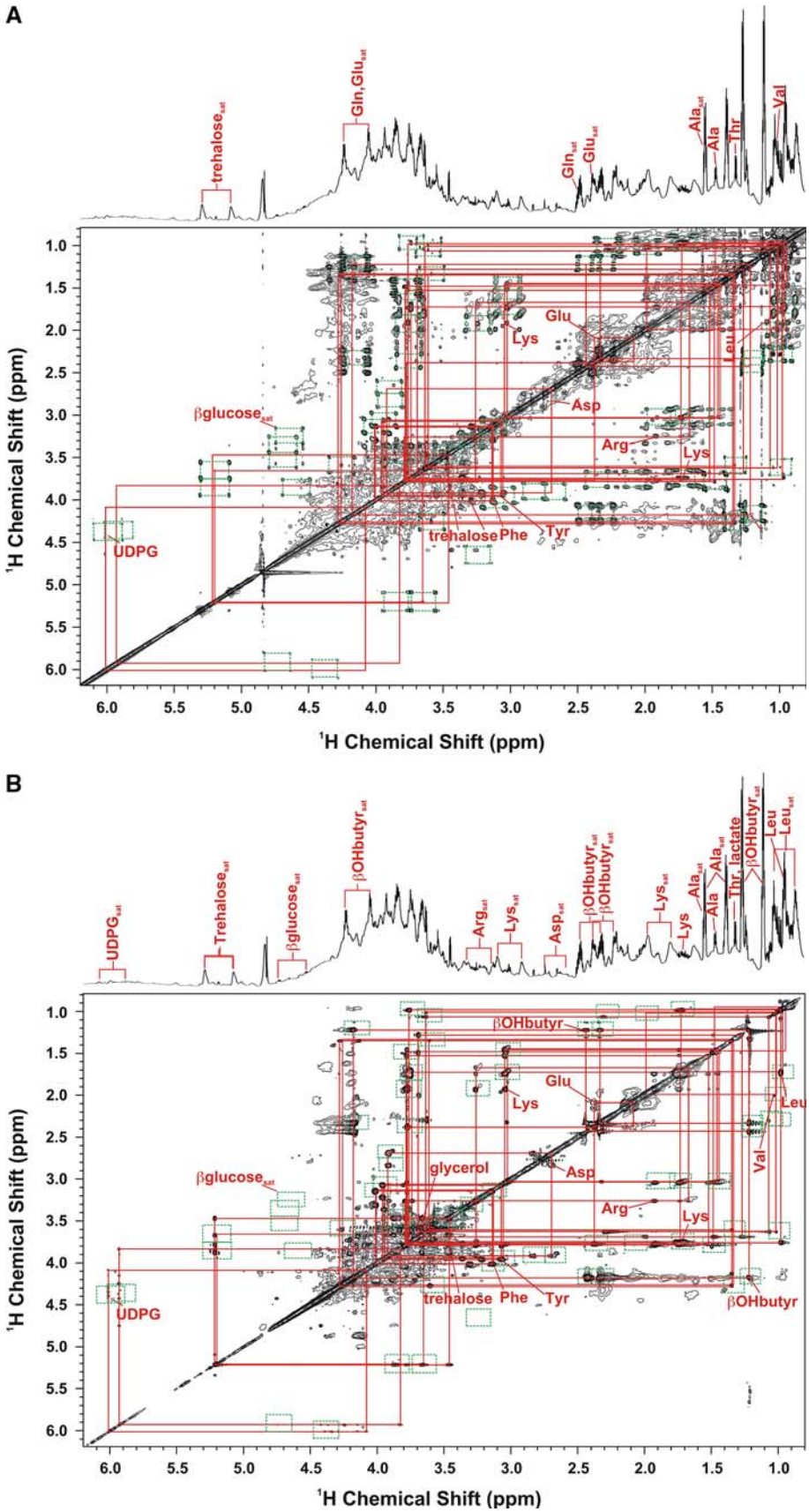

Fig. 1 2D ^{1}H TOCSY (panel **a**) and HCCH-TOCSY (panel **b**) contour maps of the polar extract of Actinobacteria isolated from the California field site. The corresponding high-resolution 1D ^{1}H NMR spectrum is shown above the 2D map. Spectra were acquired at 18.8 Tesla using a HCN triple resonance pfg probe. Solid rectangles trace the symmetric off-diagonal cross-peak patterns for various metabolites while dashed rectangles follow the split ^{13}C satellite cross-peak patterns. β-OHbutyr: β-hydroxybutyrate; metabolite$_{sat}$: ^{13}C satellites of a given metabolite

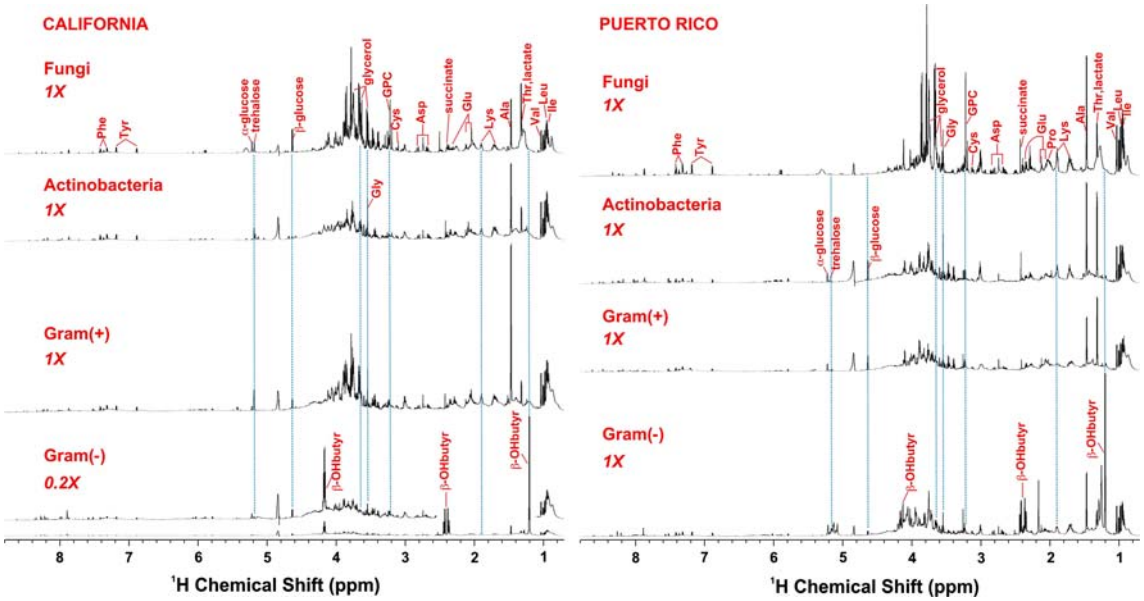

Fig. 2 1D ^{1}H NMR comparison of polar extracts for 4 groups of unlabeled microorganisms each isolated from the California and Puerto Rico field sites. The spectra were normalized to dry mass and other spectral parameters for direct comparison. The full spectrum of the Gram (−) bacterial group of the California site were scaled at 0.2× to allow proper display of the most abundant components (β-hydroxybutyrate or β-OHbutyr). The spectral insets were displayed at 1× scale. Metabolites were assigned based on their ^{1}H and ^{1}H–^{13}C covalent linkages obtained from 2D ^{1}H TOCSY and ^{1}H–^{13}C HSQC NMR experiments. GPC: glycerophosphoryl choline

microbial groups differed from each other for each site. The Gram (−) bacterial extract from California was dominated by β-hydroxybutyrate (BHB) while BHB was absent from the Fungal, Actinobacteria, and Gram (+) bacterial extracts. A high abundance of BHB was also evident in the Gram (−) bacterial extract of the Puerto Rico site while BHB was absent in the other three extracts from this site. This difference in BHB content among the different microbes could reflect their differential capacity for the β-oxidation of fatty acids.

In addition, the Fungal, Actinobacteria, and Gram (+) bacterial extracts from California contained a significant amount of trehalose whereas the Gram (−) bacterial extract was less abundant in trehalose. Overall, the trehalose content of the Puerto Rico site extracts was lower than that of the California site extracts. As trehalose is known to be a protectant against desiccation (Glasheen and Hand 1988), this difference in trehalose content could be related to a constitutive biochemical capacity for adaptation to the relatively low (California) and high (Puerto Rico) humidity conditions and higher tolerance to desiccation for the Fungal species.

To better compare the ^{13}C-enriched metabolite profiles of the different polar extracts, the extracts were analyzed by 2D high-resolution ^{13}C–^{1}H heteronuclear single quantum coherence spectroscopy (HR-HSQC). Figure 3 illustrates the HR-HSQC contour maps (b and d) along with the 1D ^{13}C projection spectra (a and c) for the Actinobacteria and Fungal extracts of the California site. The HSQC experiment revealed ^{1}H–^{13}C covalent linkages and ^{13}C spin coupling patterns (e.g. doublet and triplet for the β and α carbons of Ala, respectively). The ^{13}C spin coupling patterns enabled the determination of ^{13}C labeling at individual carbon positions, i.e. ^{13}C isotopomers for individual metabolites. For example, the doublet of Ala-Cβ and triplet of Ala-Cα arose from the coupling between ^{13}Cβ and ^{13}Cα as well as ^{13}Cα, ^{13}Cβ, and ^{13}C-carboxyl carbon, respectively, which indicates the presence of fully ^{13}C-labeled Ala. In these two maps, the ^{13}C–^{13}C spin coupling patterns for the majority of the metabolites indicates full ^{13}C enrichment, consistent with the TOCSY and HCCH-TOCSY data in Fig. 1. The ^{13}C chemical shifts and splitting patterns from the HR-HSQC analysis were used together with the ^{1}H chemical shifts and covalent linkage patterns from Fig. 1 to verify metabolite assignments.

Once assigned, the 1D ^{13}C projection spectra (Fig. 4) allowed a semi-quantitative comparison of the ^{13}C-profiles of polar extracts for the four each microbial groups from the two field sites. Because all metabolites were >95% ^{13}C-labeled at all position, the ^{13}C peak intensity reflected metabolic abundance or concentration. The profiles of microbial cell-type groups differed within the same site, i.e. each microbial group had a distinct ^{13}C isotopomer signature. When comparing the same cell-type-groups across the two sites, the Fungal groups exhibited a more consistent ^{13}C profile than the other microbial cell-type groups. In addition, the most abundant metabolites (e.g. BHB or glycerol) in each microbial group were invariably

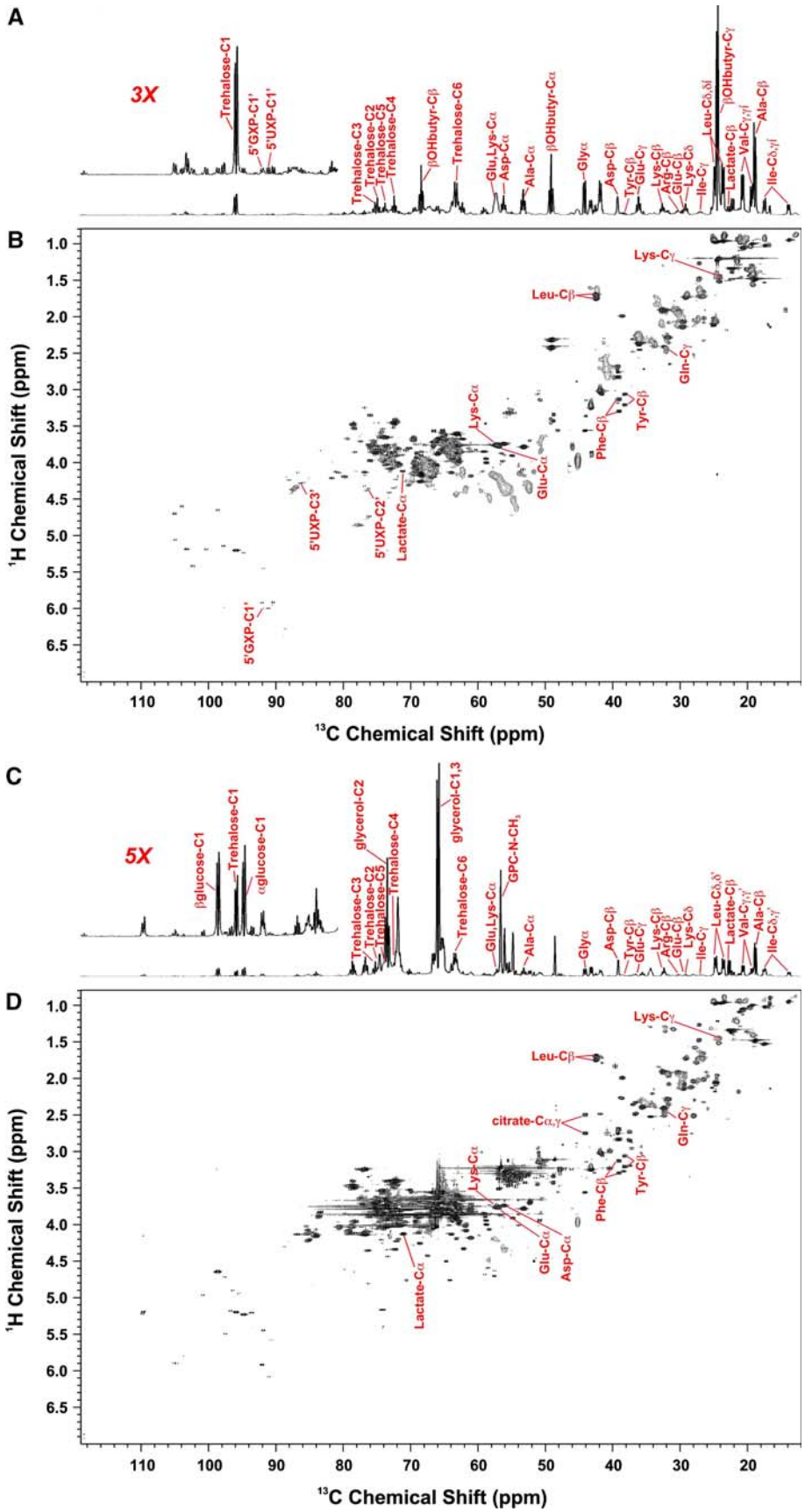

Fig. 3 2D high-resolution ^{1}H–^{13}C HSQC contour map of polar extracts of Actinobacterial (**b**) and fungal groups (**d**) isolated from the California field site. The spectra were acquired at 18.8 Tesla and 20°C with 512 increments in the ^{13}C dimension. Linear prediction to 2k points was applied to the ^{13}C dimension and the final digital points were 4k × 2k. Also shown are the 1D projection spectra (**c** for fungi and **a** for Actinobacteria) along the ^{13}C dimension. The spectral insets were displayed at 3× and 5× scale in (**a**) and (**c**), respectively. Metabolites were assigned based on their ^{1}H–^{13}C covalent linkages, ^{13}C spin coupling patterns, and reference to the ^{1}H TOCSY and ^{1}H HCCH-TOCSY data. GPC–N–CH_3: *N*-methyl carbon of gycerophosphoryl choline

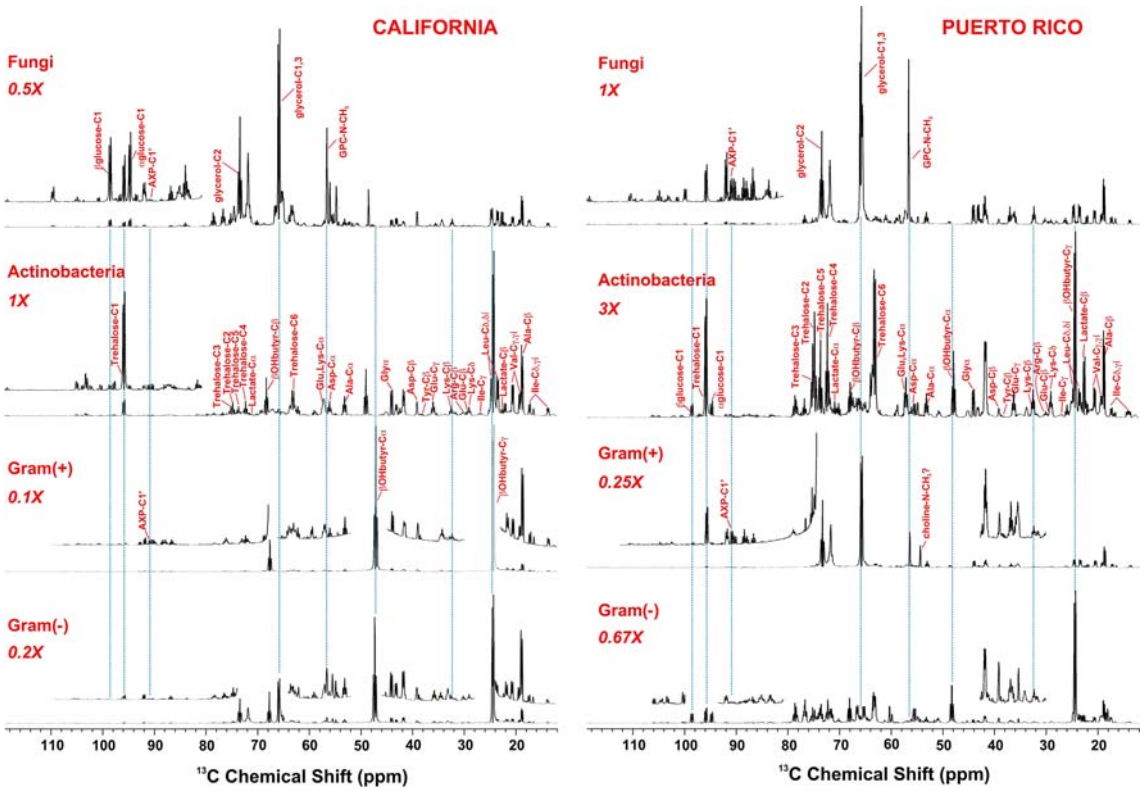

Fig. 4 1D ^{13}C HSQC projection spectra of polar extracts for 4 groups each of microorganisms isolated from the two field sites. The projection spectra were obtained from the respective 2D HSQC contour maps as in Fig. 3. The spectra were normalized to dry mass and other spectral parameters for direct comparison. Some of the full spectra were scaled differently to allow proper display of the most abundant components. The spectral insets were scaled to visualize the minor components. Metabolites were assigned as in Fig. 3. GPC–N–CH_3: *N*-methyl carbon of glycerophosphoryl choline; *β*OHbutyr: *β*-hydroxybutyrate

higher in content for microbial groups from the California site than from the Puerto Rico site.

Since these organisms were cultured in uniformly ^{13}C-labeled glucose (U-^{13}C]-glucose), ^{13}C labeling of metabolites indicates the presence of pathways for their synthesis from glucose. These include Ile, Leu, Ala, Val, lactate, BHB, Lys, Glu, Arg, Tyr, Asp, Gly, glycerol, trehalose, and adenine nucleotides (AXP). The ^{13}C-patterns and abundance (based on the intensity of the resonance in Fig. 4) of each metabolite can be used to reconstruct the biosynthetic pathways and estimate the pathway activity. For example, the Fungal groups were highly abundant in uniformly labeled glycerol ([U-^{13}C]-glycerol), which could reflect a high capacity for glycerol biosynthesis by way of glycolysis. Likewise, the dominance of [U-^{13}C]-BHB in the Gram (−) bacterial groups could be related to a high capacity for *β*-oxidation of fatty acids.

Thus, the differential ^{13}C-isotopomer profiles observed in Fig. 4 could reflect both qualitative and quantitative differences in the metabolic networks that lead to the synthesis of individual metabolites. For example, the Fungal groups had the highest synthetic capacity for glycerol. California's Fungal group maintained a higher glycerol production than the Puerto Rico's. Glycerol could serve as a osmoprotectant for desiccation or osmotic stress (Ferreira et al. 2005). As the growth medium was identical for all isolates, the higher capacity for glycerol synthesis in the Californian Fungal microbes could arise from an evolutionary adaptation to a dry Californian forests versus the humid Puerto Rican forest. This is consistent with a higher synthetic capacity for another osmoprotectant, trehalose in the Californian than in the Puerto Rican Fungal groups. Likewise, the higher [U-^{13}C]-BHB production in the California's Gram (−) bacterial group could result from a higher capacity of fatty acid *β*-oxidation than the corresponding Gram (−) bacterial group from the Puerto Rico site. It is unclear why such a basal or constitutive difference in metabolism exists for the Gram (−) bacterial group between the two sites. Perhaps, a higher energy demand from environmental adaptation and/or seasonal need for energy reserve for the California site may underlie this distinction.

It is also interesting to note the differential accumulation of [U-^{13}C]-BHB and [U-^{13}C]-glycerol in the Gram (+) bacterial group of the California and Puerto Rico sites. Again, the dominance of [U-^{13}C]-BHB for the

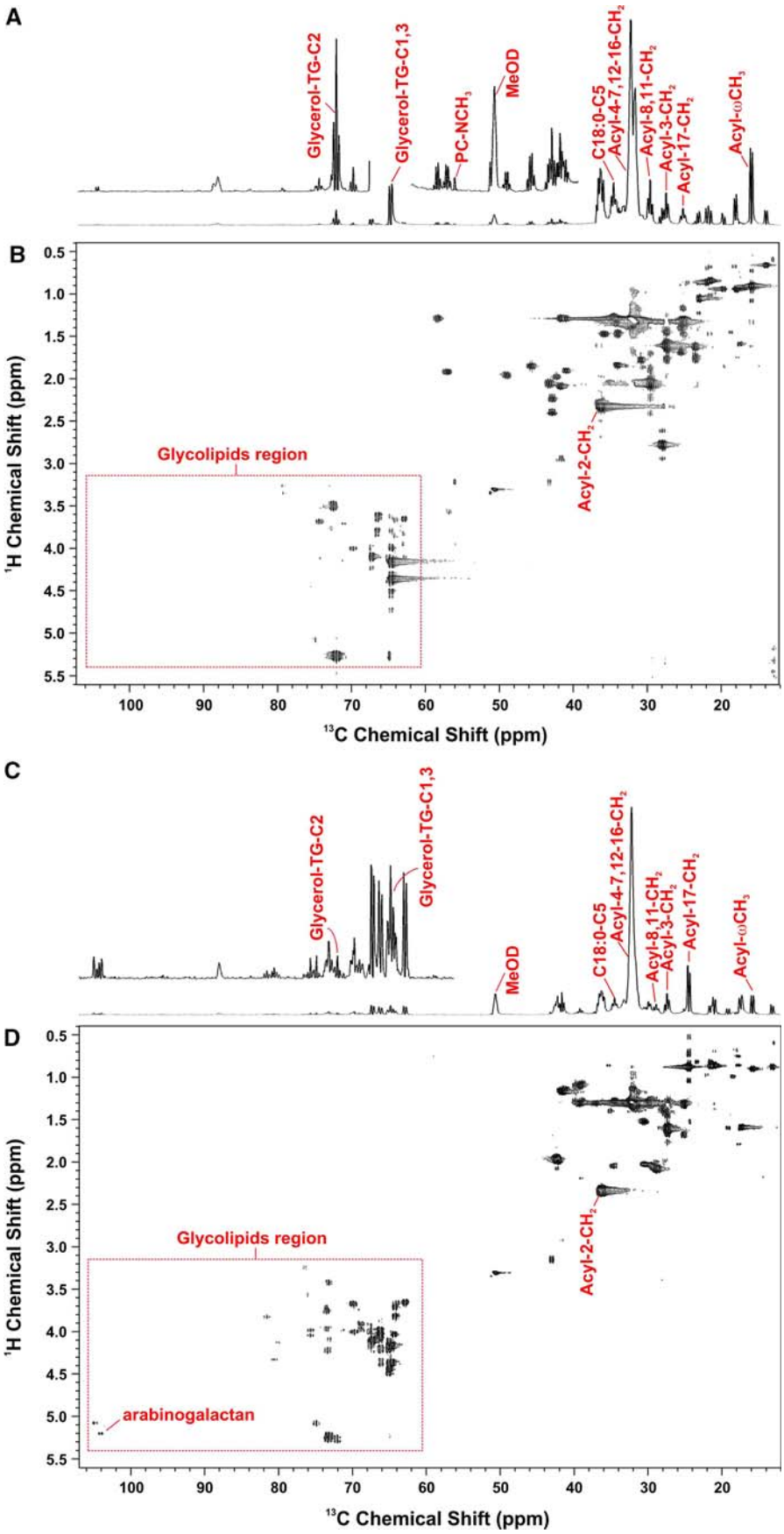

Fig. 5 2D high-resolution ^{1}H–^{13}C HSQC contour map of methanolic extracts of Actinobacterial (**b**) and Fungal groups (**d**), isolated from the Puerto Rico site. The spectra were acquired at 18.8 Tesla and processed as in Fig. 3. Also shown are the 1D projection spectra (**b** for fungi and **a** for Actinobacteria) along the ^{13}C dimension. Metabolites were assigned based on their ^{1}H–^{13}C covalent linkages, ^{13}C spin coupling patterns, and comparison with known lipid standards (Fan and Lane 2008). The arabinogalactan resonance was matched with that of 2-α-Ara*f* → 3, which is an Ara_6 motif of the arabinogalactan in the mycobacterial cell wall (Mahrous et al. 2008). PC–N–CH_3: *N*-methyl carbon of phosphatidylcholine; glycerol–TG: glycerol backbone of triglycerides; MeOD: deuterated methanol

California site suggests a high capacity for β-oxidation of fatty acids while the high abundance of glycerol could be related to a high glycolytic capacity for the Puerto Rico site. Such a dramatic difference in metabolic preference and capacity of Gram (+) bacterial group from the two sites suggests that phenetic classification may not reflect biochemical conformity and that environmental adaptation may dictate the expression of central metabolic networks in microorganisms.

3.2 Lipophilic metabolites in extracts

The same set of microbial groups form Fig. 4 was extracted with methanol to recover more polar lipid metabolites, e.g. phospholipids and glycolipids. The ^{13}C-isotopomer profiles of these extracts were analyzed by 2D high-resolution ^{1}H–^{13}C HSQC. Figure 5 illustrates the HSQC analysis for the Actinobacterial (panels a and b) and Fungal extracts (panels c and d) obtained for the Puerto Rico site. Based on the ^{1}H and ^{13}C chemical shifts, both extract spectra were abundant in triacylglycerides and glycolipids. The ^{13}C splitting patterns in the 2D contour maps (b and d) and 1D ^{13}C projection spectra (a and c) of the two extracts indicate full ^{13}C enrichment in both glyco moieties and acyl chain(s) of the glyceride lipids and glycolipids, as the case for polar extracts in Fig. 3. This is, for example, reflected by the ^{13}C doublet for the terminal methyl (ω-CH_3) group of the acyl chains and triplets for the internal methylene groups (e.g. 2,3,5,8,17-CH_2) of the acyl chains. Moreover, the Fungal extract was relatively more abundant in glycolipids relative to the Actinobacterial extract. In particular, an anomeric resonance tentatively assigned to arabinogalactan (Mahrous et al. 2008) in the Fungal extract (Fig. 5c, d) was absent in the Actinobacterial extract (Fig. 5a, b). Arabinogalactan is known to be a component of a highly diverse cell surface proteins in plants (Seifert and Roberts 2007) and of lipopolysaccharides in some Actinobacteria such as Mycobacterium (Mahrous et al. 2008).

For a semi-quantitative comparison of the ^{13}C content (and thus concentration) in lipophilic metabolites, the 1D ^{13}C projection spectra of the 4 each microbial cell-type groups from the two field sites were plotted and shown in

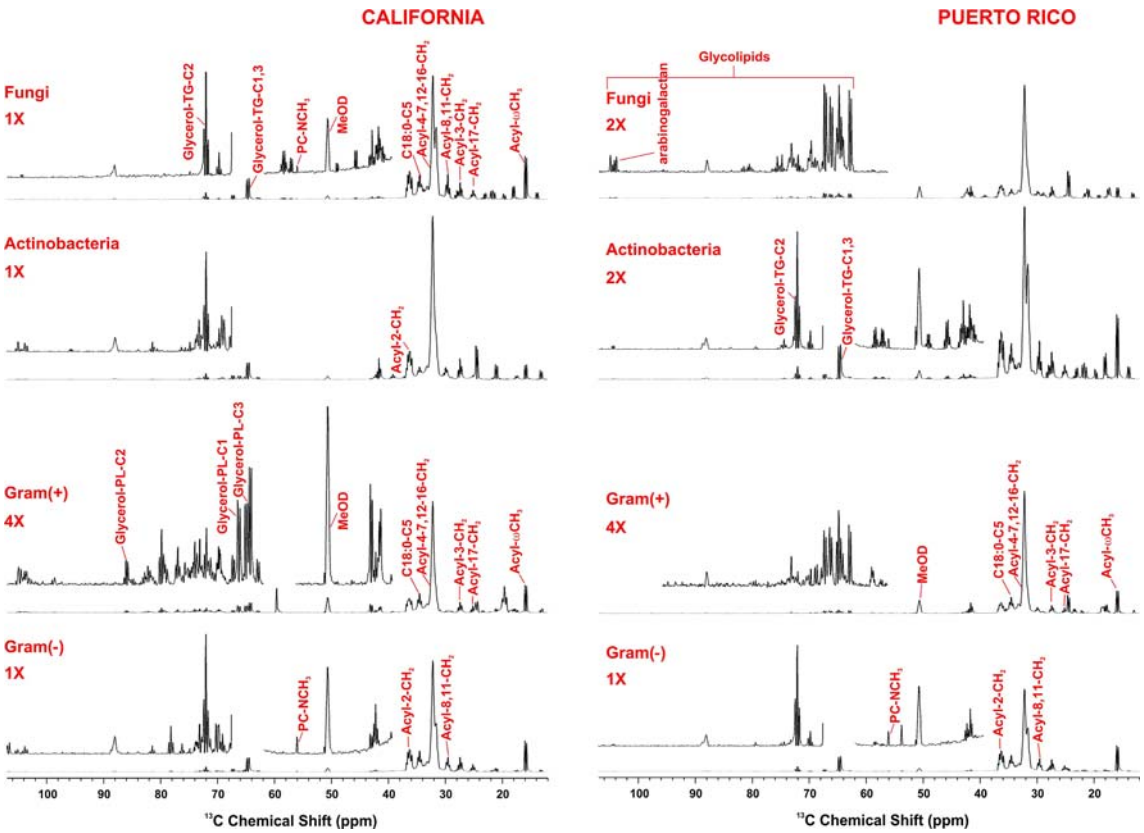

Fig. 6 1D ^{13}C HSQC projection spectra of methanolic extracts for 4 groups of microorganisms isolated from the two field sites. The projection spectra were obtained from the respective 2D HSQC contour maps as illustrated in Fig. 5. The spectra were normalized to dry mass and other spectral parameters for direct comparison. Some of the full spectra were scaled differently to allow proper display of the most abundant components. The spectral insets were scaled to visualize the minor components. Lipid metabolites were tentatively assigned based on their ^{1}H and ^{13}C chemical shifts. PC–N–CH_3: *N*-methyl carbon of phosphatidylcholine; TG: triacylglycerides; PL: phospholipids; MeOD: deuterated methanol

Fig. 6. As the case for the polar metabolites (cf. Fig. 4), the microbial groups of the California site had consistently higher ^{13}C content in many lipophilic metabolites than the Puerto Rico site (Fig. 6). Taken together, these results suggest that the Californian microbes had a higher basal metabolic capacity than the Puerto Rican counterparts, when grown under standard laboratory conditions. Composite variations in lipophilic metabolites were also observed within and between the two sites. Based on the relative peak intensity of the ^{13}C-labeled glycerol backbone, the Gram (+) bacterial biomass was more enriched in phospholipids (PL) while the other three composites were higher in ^{13}C-labeled triacylglycerides (TG) for both sites (Fig. 6). The Gram (+) bacterial group of the two sites also had a relatively higher ^{13}C intensity in the resonances of the glycosyl region of the HSQC projection spectra. These data could reflect a higher capacity of PL and glycolipid synthesis in the Gram (+) bacterial group.

3.3 In situ metabolite analysis

In addition to the analysis of microbial extracts, the intact lyophilized biomass of microbial groups from the two field sites were analyzed by NMR at 18.8 T in the solid-state mode. Using cross-polarization and magic angle spinning (CP-MAS), ^{13}C NMR spectra of the ^{13}C-enriched composites were acquired with good signal-to-noise in 43 min. The high ^{13}C enrichment also enabled 2D solid-state ^{13}C–^{13}C correlation spectra to be acquired with ca. 17–22 mg each of the lyophilized groups. Figure 7 displays the 2D data for the Gram (−) bacterial group from the Puerto Rico site (panel c) and Actinobacteria from the California site (panel f). Also shown are the corresponding 1D projection and 1D CP-MAS spectra. The solid-state ^{13}C spectra of the Actinobacterial group contained mainly the relatively sharp resonances of the acyl and glycosyl carbons, which were tentatively assigned based on the ^{13}C–^{13}C coupling patterns. The three prominent broad resonances in Fig. 7a (26, 48, and 73.9 ppm) arise from three covalently linked carbons as demonstrated by the cross peak patterns in Fig. 7c. Their chemical shifts were similar but not identical to those of the three ^{13}C resonances of BHB in the corresponding polar extract in Fig. 8. Moreover, these broad resonances were absent in the polar extract spectrum, which suggests the corresponding metabolite was not extracted by polar solvents. Thus, the three broad resonances in the intact samples were assigned to poly(BHB), which is consistent with the reported abundance of poly(BHB) in Gram (−) bacteria (Sangkharak and Prasertsan 2008; Steinbüchel 2001).

Similar acyl carbon coupling patterns were evident in the correlation map of the Puerto Rico's Gram (−) bacterial group (Fig. 7c). However, this map also shows three dominant and broad resonances at 26, 48, and 74 ppm, which were correlated with each other and with resonances at 101 (anomeric), 112 (aromatic), 121.8 (olefinic), and

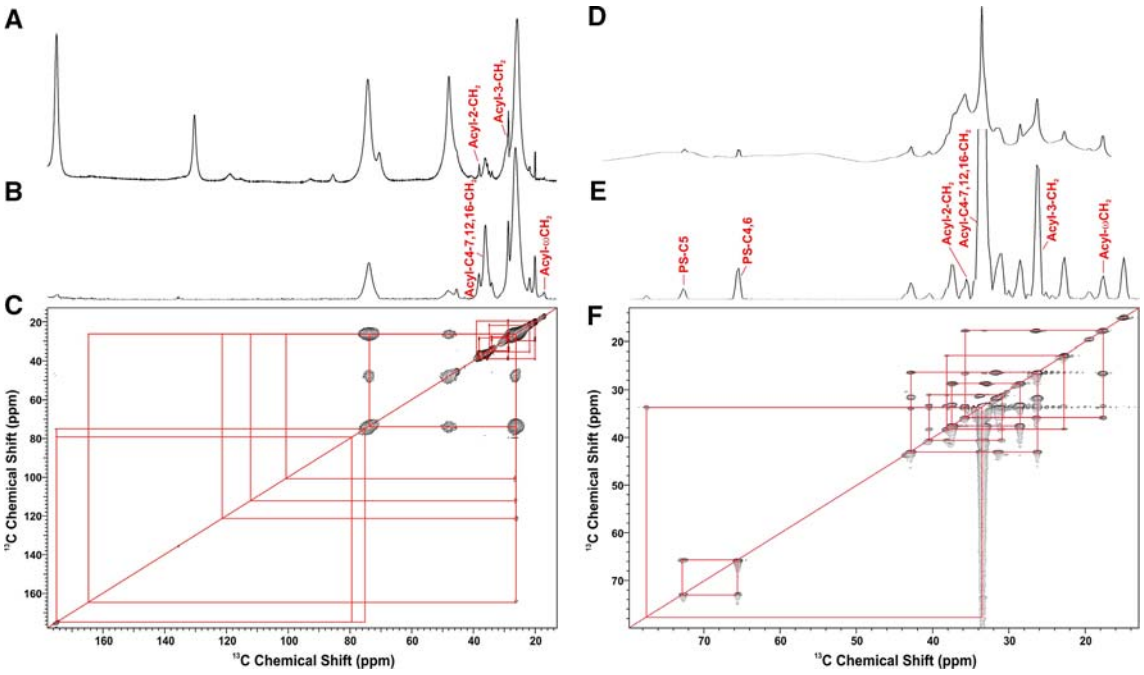

Fig. 7 2D solid-state CP-MAS ^{13}C correlation contour map of Gram (−) bacterial group (panel **c**) from Puerto Rico site and Actinobacteriaal group from the California site (panel **f**). Also shown above the 2D map are the corresponding 1D projection spectra (**b**, **e**) and 1D CP-MAS spectra (**a**, **d**). All spectra were acquired at 18.8 T with a 9 kHz spinning rate at the magic angle and with cross-polarization transfer. Each set of off-diagonal cross peaks (traced by rectangles) in panel **c** represents ^{13}C–^{13}C covalent linkages

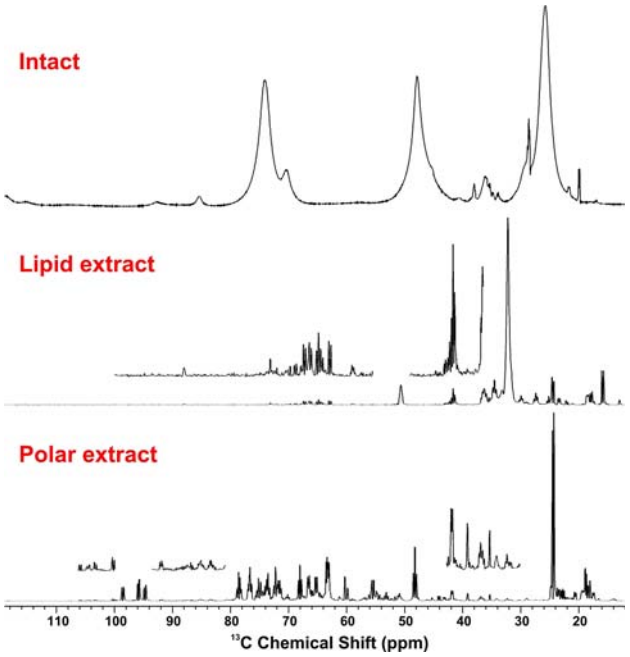

Fig. 8 Comparison of ^{13}C NMR spectra of intact biomass with those of polar and lipid extracts of Gram (−) bacterial group isolated from the Puerto Rico site. The spectra for the intact biomass from this figure, polar extract and lipid extract was from Figs. 4 and 6

164.5 ppm (carboxylic ester), although the latter four resonances were barely visible. The carbon covalent linkage patterns represented by these resonances suggest the presence of glycolipids with aromatic group(s) and unsaturated acyl chain(s). The broad linewidth and/or weak intensity of these resonances could reflect a less dynamic environment for the corresponding carbons than other acyl carbons of the same group or acyl and glycosyl carbons of the Actinobacterial group from the California site. Also noted was the distinct appearance of the ^{13}C NMR spectra acquired from intact biomass under solid-state conditions versus those acquired from the corresponding polar and lipid extracts, as illustrated for Puerto Rico's Gram (−) bacterial group in Fig. 8. This distinction could result from the influence of molecular motion on the observability of metabolite resonances in the solid-state and/or dominance of resonances of non-extracted components (e.g. glycoproteins) in the intact biomass spectrum.

To compare the carbon signature of all eight cell-type groups, their 1D CP-MAS ^{13}C NMR spectra were acquired and displayed in Fig. 9. The ^{13}C spectral signature of the four microbial groups from each site differed among each other, reflecting fundamental differences in their physiologies and morphologies. Interestingly, the Fungal group signature resembled more the Actinobacterial group signature than the signatures of Gram (+) and Gram (−) bacterial groups, and vice versa. It is also important to note that similar microbial composites (e.g. Fungal groups) displayed comparable ^{13}C signatures across the two sites, albeit with some site differences. Thus, similar types of

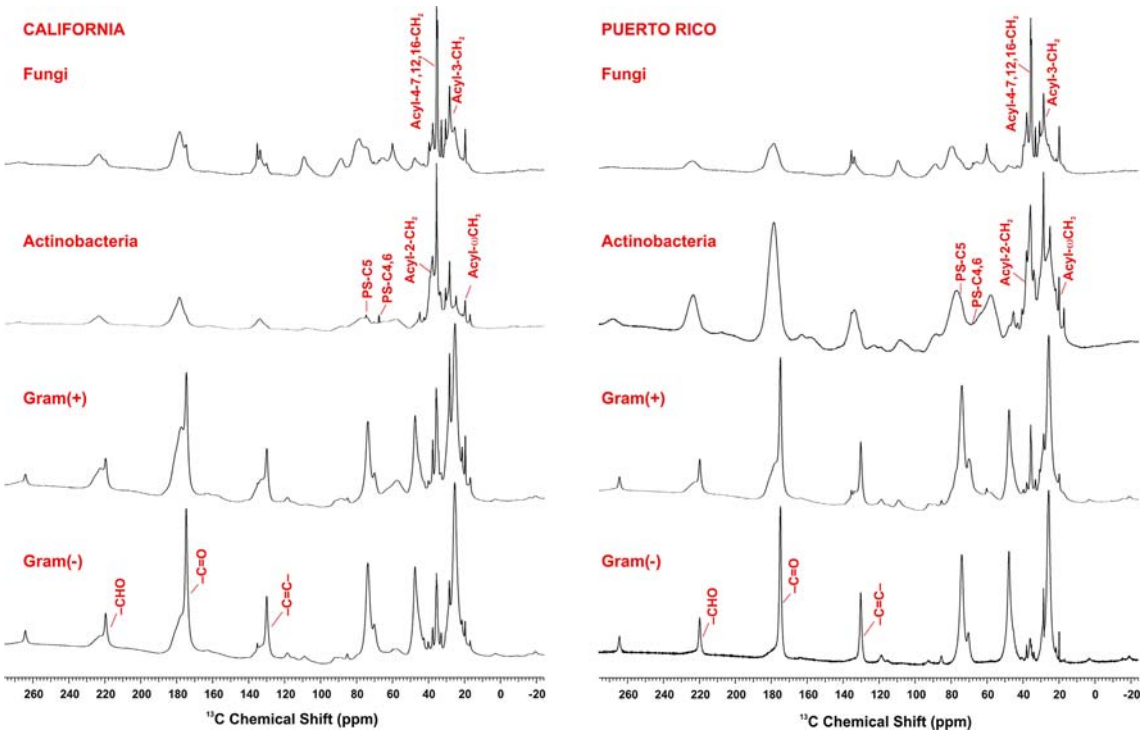

Fig. 9 1D solid-state CP-MAS ^{13}C NMR spectra of four each microbial group from the California and Puerto Rico sites. All spectra were acquired at 18.8 Tesla with a 9 kHz spinning rate at the magic angle and with cross-polarization transfer. PS: polysaccharides

microbes may share common biochemical traits, which can be explored for functional classification to complement genetics or morphology-based classification schemes.

More importantly, the ^{13}C-metabolite signatures presented in Figs. 4, 6 and 8 reflect the ability of each microbial group to metabolize glucose, from which glucose-associated metabolic networks may be reconstructed. Other metabolic networks can also be reconstructed using appropriate stable isotopic tracers. Such network knowledge can serve as a powerful tool for genome-wide annotation of gene functions. This can, in turn, promote a systematic and molecular-level understanding of indigenous microbial functions whether they be contributions to biogenic CO_2 production, adaptation to different ecological niches or interactions with host organisms in a beneficial or pathogenic capacity. However, it should also be noted that many of the site-dependent metabolic traits may be lost under standard laboratory culture conditions. These adaptive traits will need to be addressed by direct field experimentation and/or laboratory simulation studies.

Acknowledgments This work was supported by NSF grants DEB0343577 and EPS-0447479. NMR spectra were recorded at the J.G. Brown Cancer Center NMR facility. Part of this work was performed under the auspices of the U.S. Department of Energy by the University of California, Lawrence Berkeley National Laboratory, under contract DE-AC02-05CH11231. We thank T. Shimada, E. Long and J. Fortney for their assistance with the microbial isolation, screening and culture of the microorganisms; and S. Arumugam for help with solid state NMR. We also thank Drs. Mary Firestone and Richard Higashi for helpful discussion.

References

Alef, K. (1995). *Nutrients, sterilization, aerobic and anaerobic culture techniques*. San Diego, USA: Academic Press Inc.

DeSantis, T. Z., Hugenholtz, P., Larsen, N., Rojas, M., Brodie, E. L., Keller, K., et al. (2006). Greengenes, a chimera-checked 16S rRNA gene database and workbench compatible with ARB. *Applied and Environmental Microbiology, 72*, 5069–5072. doi:10.1128/AEM.03006-05.

Eswaran, H., Van den Berg, E., & Reich, P. (1993). Organic carbon in soils of the world. *Soil Science Society of America Journal, 57*, 192–194.

Fan, T., Bandura, L., Higashi, R., & Lane, A. (2005). Metabolomics-edited transcriptomics analysis of Se anticancer action in human lung cancer cells. *Metabolomics Journal, 1*, 325–339. doi:10.1007/s11306-005-0012-0.

Fan, T. W.-M., Higashi, R. M., & Lane, A. N. (2006). Integrating metabolomics and transcriptomics for probing Se anticancer mechanisms. *Drug Metabolism Reviews, 38*, 707–732. doi:10.1080/03602530600959599.

Fan, T. W.-M., & Lane, A. N. (2008). Structure-based profiling of Metabolites and Isotopomers by NMR. *Progress in Nuclear Magnetic Resonance Spectroscopy, 52*, 69–117. doi:10.1016/j.pnmrs.2007.03.002.

Fan, T. W.-M., Lane, A. N., Chekmenev, E., Wittebort, R. J., & Higashi, R. M. (2004). Synthesis and physico-chemical properties of peptides in soil humic substances. *The Journal of Peptide Research, 63*, 253–264. doi:10.1111/j.1399-3011.2004.00142.x.

Ferreira, C., van Voorst, F., Martins, A., Neves, L., Oliveira, R., Kielland-Brandt, M. C., et al. (2005). A Member of the Sugar Transporter Family, Stl1p Is the Glycerol/H+Symporter in Saccharomyces cerevisiae. *Molecular Biology of the Cell, 16*, 2068–2076. doi:10.1091/mbc.E04-10-0884.

Gardes, M., & Bruns, T. D. (1993). ITS primers with enhanced specificity for basidiomycetes—application to the identification of mycorrhizae and rusts. *Molecular Ecology, 2*, 113–118. doi:10.1111/j.1365-294X.1993.tb00005.x.

Glasheen, J. S., & Hand, S. C. (1988). Anhydrobiosis in embryos of the brine shrimp Artemia: Characterization of metabolic arrest during reductions in cell-associated water. *The Journal of Experimental Biology, 135*, 363–380.

Kögel-Knabner, I. (2002). The macromolecular organic composition of plant and microbial residues as inputs to soil organic matter. *Soil Biology and Biochemistry, 34*, 139–162. doi:10.1016/S0038-0717(01)00158-4.

Lane, A. N., & Fan, T. W.-M. (2007). Quantification and identification of isotopomer distributions of metabolites in crude cell extracts using 1H TOCSY. *Metabolomics, 3*, 79–86. doi:10.1007/s11306-006-0047-x.

Lane, A. N., Fan, T. W.-M., & Higashi, R. M. (2008). Isotopomer-based metabolomic analysis by NMR and mass spectrometry. *Methods in Cell Biology, 84*, 541–588. doi:10.1016/S0091-679X(07)84018-0.

Lane, D. J., Pace, B., Olsen, G. J., Stahl, D. A., Sogin, M. L., & Pace, N. R. (1985). Rapid determination of 16S ribosomal RNA sequences for phylogenetic analyses. *Proceedings of the National Academy of Sciences of the United States of America, 82*, 6955–6959. doi:10.1073/pnas.82.20.6955.

Mahrous, E. A., Lee, R. B., & Lee, R. E. (2008). A rapid approach to lipid profiling of mycobacteria using 2D HSQC NMR maps. *Journal of Lipid Research, 49*, 455–463. doi:10.1194/jlr.M700440-JLR200.

Meyers, R. T., Zak, D. R., White, D. C., & Peacock, A. (2001). Landscape-level patterns of microbial community composition and substrate use in upland forest ecosystems. *Soil Science Society of America Journal, 65*, 359–367.

Post, W. M., Emanuel, W. P., Zinke, P. J., & Stangenberger, G. (1982). Soil carbon pools and world life zones. *Nature, 298*, 156–159. doi:10.1038/298156a0.

Saetre, P., & Bååth, E. (2000). Spatial variation and patterns of soil microbial community structure in a mixed spruce-birch stand. *Soil Biology and Biochemistry, 32*, 909–917. doi:10.1016/S0038-0717(99)00215-1.

Sangkharak, K., & Prasertsan, P. (2008). Nutrient optimization for production of polyhydroxybutyrate from halotolerant photosynthetic bacteria cultivated under aerobic-dark condition. *Electronic Journal of Biotechnology, 11*. Available from Internet: http://www.ejbiotechnology.cl/content/vol11/issue3/full/2/index.html.

Schlesinger, W. H. (1977). Carbon balance in terrestrial detritus. *Annual Review of Ecology and Systematics, 8*, 51–81. doi:10.1146/annurev.es.08.110177.000411.

Seifert, G. J., & Roberts, K. (2007). The biology of arabinogalactan proteins. *Annual Review of Plant Biology, 58*, 137–161. doi:10.1146/annurev.arplant.58.032806.103801.

Staff, S. S. (1999). *Soil taxonomy. A basic system of soil classification for making and interpreting soil surveys. USDA Natural Resource Conservation Service Agriculture Handbook # 436* (2nd ed.). Washington, DC: US Government Printing Office.

Steinbüchel, A. (2001). Perspectives for biotechnological production and utilization of biopolymers: Metabolic engineering of

polyhydroxyalkanoate biosynthesis pathways as a successful example. *Macromolecule Bioscience, 1*, 1–24.

Taylor, R. E. (2004). Setting up C-13 CP/MAS experiments. *Concepts in Magnetic Resonance Part A, 22A*, 37–49. doi:10.1002/cmr.a.20008.

Waldrop, M. P., & Firestone, M. K. (2003). Altered utilization patterns of young and old soil C by microorganisms caused by temperature shifts and N additions. *Biogeochemistry, 67*, 235–268. doi:10.1023/B:BIOG.0000015321.51462.41.